Asymptotic Analysis of Compound Volume+Shape Metrics for Mesh Optimization*

Veselin A. Dobrev† Patrick Knupp‡ Tzanio Kolev† Ketan Mittal†
Robert N. Rieben† Michael Stees† Vladimir Z. Tomov†§

Abstract

Mesh optimization metrics of type Volume+Shape (VS) are critical in controlling local volume, skew, and aspect ratio in computational meshes. Such metrics can be viewed as being intermediate between pure shape metrics and pure volume metrics. In most applications using VS metrics one wants the optimal mesh to display a good balance between shape and volume characteristics. Many existing VS metrics are shape-dominated or volume-dominated, meaning that they do not give good balance between shape and volume. To achieve balance, some of the existing VS metrics contain a user parameter to adjust the balance in one direction or the other. Unfortunately this parameter is currently determined by trial and error because the parameter is not intuitively linked to a definition of balance. In this work we study the asymptotic properties of different compound metrics and find the ones that provide good balance between shape and volume. This asymptotic approach is motivated, presented, and tested by numerical experiments. The experiments confirm the expected behavior of the metrics and yields volume-shape balance in the optimized mesh.

1 Introduction

Geometric mesh quality refers to those geometric properties of a mesh and its elements which impact robustness, efficiency, and accuracy of a physical or engineering simulation [13, 10, 12, 3]. Four of the most important geometric properties are local volume/area, orientation, skew, and aspect ratio. While the connection between geometric quality of a mesh and its impact on a physical simulation is not completely understood, it is generally accepted that the local volume/area should be positive, skew should not be extreme (i.e., no small or large angles), and aspect ratio should be suitable to the problem at hand. Meshes which suffer from defects related to these issues can often be repaired by mesh optimization techniques, including that of node-movement [22, 21, 23, 8]. A particular method of node movement that is discussed in this work is the Target Matrix Optimization Paradigm (TMOP) [14, 8]. Distinctive features of TMOP include the use of sample points, target-matrices [17, 16], Jacobian-weighted local quality metrics [18], and a theory of metric type [15]. There are three primary metric types: shape (S), volume+shape (VS) [1] , and volume+orientation+shape (VOS). These names signify the particular aspects of geometric mesh quality that the metric is intended to control or improve. For example, a VS metric allows, in principle, the user to improve the local volume/area at sample points in the mesh and simultaneously improve the local shape.

1.1 Notation We briefly go over the TMOP notions that are relevant to this work. The matrix $W_{d\times d}$ is the Jacobian of the transformation from the *reference* to the *target* coordinates, where d is the dimension. This matrix is defined according to a user-specified method prior to optimization; it defines the desired local properties of the optimal mesh. The matrix $A_{d\times d}$ is the Jacobian of the transformation between the *reference* and *physical* space coordinates, i.e., it describes the local properties of the actual mesh that is being optimized. Then $T = AW^{-1}$ represents the transformation from the *target* configuration to the *physical* mesh positions; this matrix is used to measure mesh quality. We denote $\det(T) = \tau$ and $\det(A) = \upsilon$.

The local mesh quality is measured by a scalar function $\mu(T) \geq 0$. Depending on the specific formula for μ, mesh quality is measured with respect to different geometric parameters, e.g., formulas based exclusively on τ represent volume (V) metrics, which are invariant to aspect ratio, skew and rotation; see [15] for further details, metric types, and specific metric formulas.

*Performed under the auspices of the U.S. Department of Energy under Contract DE-AC52-07NA27344 (LLNL-CONF-853493).

†Lawrence Livermore National Laboratory, Livermore, CA, U.S.A. {dobrev1,kolev1,mittal3,rieben1,stees1,tomov2}@llnl.gov.

‡Dihedral LLC, Bozeman, MT, U.S.A. knupp.patrick@gmail.com.

§Corresponding Author.

[1] The VS metric type is also often called Shape+Size.

1.2 Statement of the Problem A linear compound VS metric is formed by choosing one shape metric and one volume metric. A user parameter $\gamma \in (0,1)$ creates a convex combination VS metric μ_{vs} of the form

$$\mu_{vs} = (1-\gamma)\,\mu_s + \gamma\,\mu_v, \tag{1.1}$$

where μ_s stands for one of the shape metrics and μ_v for one of the volume metrics used in TMOP.

The problem is independent of dimension, but it's easier to demonstrate in 2D. In TMOP the most commonly used 2D shape metrics are

$$\mu_{2,s} = \frac{|\,T\,|^2}{2\,\tau} - 1,$$

$$\mu_{50,s} = \frac{|\,T^tT\,|^2}{2\,\tau^2} - 1,$$

$$\mu_{51,s} = \frac{|TT^tT|^2}{2\,\tau^3} - 1,$$

$$\mu_{58,s} = \left|\frac{T^tT}{\tau} - I\right|^2,$$

while the three most commonly used volume metrics are

$$\mu_v \;=\; \frac{1}{2}\left(\tau^p - \tau^{-p}\right)^2 = \frac{1}{2}\left(\tau^{2\,p} + \tau^{-2\,p}\right) - 1$$

with $p \in \left\{\frac{1}{2}, 1, \frac{3}{2}\right\}$. The metric with $p = \frac{1}{2}$ is denoted by $\mu_{56,v}$, $p = 1$ is denoted by $\mu_{77,v}$, and $p = \frac{3}{2}$ is denoted by $\mu_{20,v}$. With the four shape metrics and the three volume metrics just defined, there are 12 combinations of μ_s and μ_v resulting in a linear compound VS metric. These are shown in Table 1, with metric numbers assigned to each combination.

	$\mu_{56,v}$	$\mu_{77,v}$	$\mu_{20,v}$
$\mu_{2,s}$	$\mu_{94,vs}$	$\mu_{80,vs}$	$\mu_{16,vs}$
$\mu_{50,s}$	$\mu_{53,vs}$	$\mu_{90,vs}$	$\mu_{19,vs}$
$\mu_{51,s}$	$\mu_{75,vs}$	$\mu_{76,vs}$	$\mu_{49,vs}$
$\mu_{58,s}$	$\mu_{59,vs}$	$\mu_{78,vs}$	$\mu_{65,vs}$

Table 1: Twelve Linear Compound VS Metrics with Parameter γ.

For each of the twelve VS metrics, the parameter γ forms a family of metrics μ_{vs}. For γ near 0, μ_{vs} generally creates optimal meshes with features similar to meshes created by optimizing a shape metric. For γ near 1, μ_{vs} generally creates optimal meshes with features similar to meshes created by optimizing a volume metric. In principle, γ near $\frac{1}{2}$ should create optimal meshes with features similar to both shape and volume metrics. In practice this is not necessarily the case. Depending on the mesh connectivity and on the particular VS metric employed, one often needs to make γ as small as 0.2 or as large as 0.8 to obtain an optimal mesh with good balance between shape and size. Finding the value of γ that gives the best balance between shape and volume has been to date a trial and error process which must be performed for each particular mesh that one wants to optimize. Thus, the problem addressed in this work is to *find compound VS metrics that asymptotically balance shape and volume, and determine a-priori the best values for γ, without user intervention.* This problem has been partly discussed in [6], where the authors derive trade-off parameters between shape and volume, in the context of mesh generation for a specific 2D horseshoe domain.

An optimal mesh created by a VS metric that shows too much shape influence can be characterized by: 1) large *pull-away* from concave areas and/or 2) mesh elements with a wide range of areas even when the target matrix is constant. By *pull-away* we mean that mesh lines (in block-structured meshes) tend to pull away from concave boundaries or internal interfaces. Often element areas are very small in parts of the domain with convex boundaries or at tri-valent nodes. Optimal meshes created by VS metrics with these features are called *shape-dominated*. Even with unstructured meshes, shape-dominance can sometimes be observed.

An optimal mesh created by a VS metric that shows too much volume influence can be characterized by 1) elements with too much skew, 2) high aspect ratio elements, or 3) a general lack of smoothness. Optimal meshes created by VS metrics with these features are called *volume-dominated*. An optimal mesh with minor pull-away, a reasonably small range of element areas, minor skew, non-extreme aspect ratios, and having a smooth appearance is said to be a *visually balanced* optimal mesh. Such meshes can be created using VS metrics provided γ has been selected appropriately.

1.3 Examples of Balanced and non-Balanced Optimal Meshes from VS Metrics Two optimal meshes having the same number of elements on the same domain are shown in Figure 1. The mesh on the left was obtained by optimizing the shape metric $\mu_{2,s}$ and the mesh on the right from optimizing volume metric $\mu_{56,v}$. Both of these meshes are likely unsuitable for computation. The optimal mesh from the shape metric shows severe *pull-away*, in which the vertical mesh lines do not follow the right boundary very closely. The optimal mesh from the volume metric produces elements of approximately the same area, but with more skew than in the shape-dominated mesh. Thus, neither of

the two meshes show good visual balance nor are they expected to. Balance can only be achieved using a VS metric with the correct value of γ.

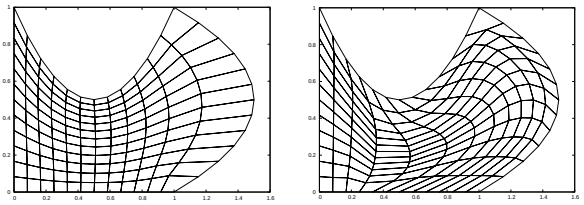

Figure 1: Optimal Meshes for Shape Metric $\mu_{58,s}$ (left) and Volume Metric $\mu_{77,v}$ (right).

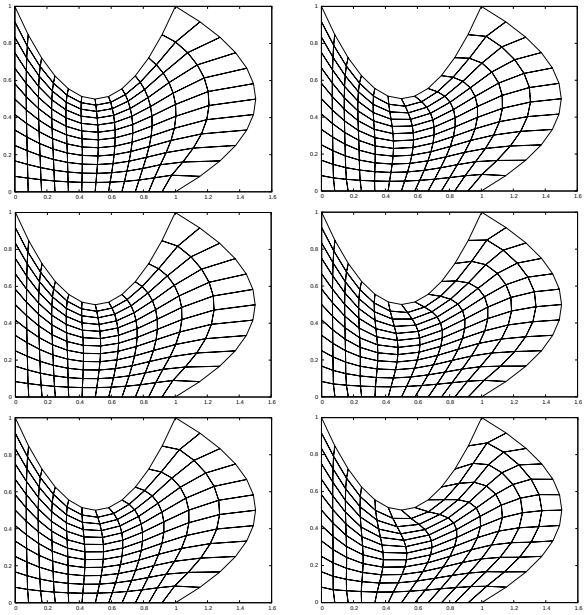

Figure 2: Optimal Meshes for $\mu_{78,vs}$ with increasing γ.
Left Column (top to bottom): $\gamma = \frac{1}{7}, \frac{2}{7}, \frac{3}{7}$.
Right Column (top to bottom): $\gamma = \frac{4}{7}, \frac{5}{7}, \frac{6}{7}$.

Figure 2 shows optimal meshes obtained from optimizing with VS metric $\mu_{78,vs} = (1-\gamma)\,\mu_{58,s} + \gamma\,\mu_{77,v}$ for an increasing sequence of six values of γ. With $\gamma = \frac{1}{7}$, the optimal mesh is strongly shape dominated, as seen by the pull-away on the right. As γ increases, the area of the elements in the mesh gradually become more equal. Visually, the meshes created from $\gamma = \frac{4}{7}$ to $\frac{5}{7}$ are getting closer to being balanced between shape and volume. Balance does not occur with $\gamma = \frac{1}{2}$, but with a larger value of γ. It is this effect that makes it difficult to find the correct value of γ without trial and error.

1.4 Further considerations and requirements Generally, the ratio between the magnitudes of the metrics μ_s and μ_v does not have a clear geometric meaning. For example, $\mu_s(x) = 10$ may be produced by a point x where the local aspect ratio is 1.2 times different than the target one, while $\mu_v(x) = 10$ may be produced by a point x where the local size is 5 times larger than the target size. Although in this case the magnitudes are perfectly balanced with $\mu_s(x) = \mu_v(x)$, the size-quality at the point x is much worse. This suggests that balancing the metrics' magnitudes is not always the best approach.

Furthermore, many mesh optimization approaches [21, 23, 8] solve a nonlinear problem with respect to the derivatives of (1.1) to obtain the optimal mesh, for example

$$\frac{\partial}{\partial x} \int_{\Omega} \left[(1-\gamma)\,\mu_s(x) + \gamma\,\mu_v(x) \right] = 0. \tag{1.2}$$

For such solvers it is more appropriate to consider balancing the derivatives of μ_s and μ_v, instead of their magnitudes.

Finally, we pose the requirement that the optimal value of γ should be fixed throughout the mesh optimization process. The issue of using dynamic γ is that iterative solvers would be getting a different objective function, e.g. (1.2), at every γ update, which makes the notion of convergence more complex.

1.5 Proposed approach In this work we examine the behavior of various μ_s and μ_v metrics in terms of asymptotic limits of the geometric parameters, i.e., we examine their values when these parameters approach their extreme values. Knowing the asymptotic behavior of the μ_s and μ_v components, for each specific composite metric we derive a universal scaling constant which is independent of the specific mesh in use. By employing asymptotically balanced metrics, both terms of the composite metric undergo proportional changes under similar shape and size deformations. Balanced volume+shape metrics will be highly beneficial in the context of size-adaptive mesh optimization [9, 20, 11, 19, 7, 4, 5], as such methods must always consider the balance between local size accuracy and shape quality.

The rest of the paper has the following organization. In Section 2 we derive asymptotically balanced 2D VS metrics, while the 3D case is considered in Section 3. General theory about compound TMOP metrics of any type is presented Section 4. In Section 5 we present some application examples that use the derived balanced metrics. Finally, we close with conclusions and directions for future work in Section 6.

2 Compound Metrics for 2D Elements

First consider the case of compound metrics for 2D mesh elements. The relevant geometric parameters are skew (ϕ), lengths (a and b), and volume (υ). With no loss of generality, we set $a = 1$. To simplify the presentation of the main idea, we assume $W = I$, i.e, $T = A$ and $\tau = \upsilon$. The case $W \neq I$ is discussed in Section 2.1.

Since VS metrics are invariant of rotation, we shall assume that the angle of rotation is zero. In terms of the remaining geometric parameters, the Jacobian matrix is

$$A = \begin{pmatrix} 1 & b\cos\phi \\ 0 & b\sin\phi \end{pmatrix}.$$

From this, we see that $\upsilon = det(A) = b\sin\phi$. Also, $|A|^2 = 1 + b^2$.

Extreme values of the volume metrics are reached when either $\upsilon \to \infty$ or $\upsilon \to 0$. For $\upsilon \to \infty$, it must be that $b \to \infty$. On the other hand, if $\upsilon \to 0$, there are two possibilities: either $b \to 0$, or $\sin\phi \to 0$. Table 2 summarizes the limiting cases to consider. Note that, in Table 2, selecting a specific finite value for a geometric parameter (e.g. $b = 1$) is not of utmost significance; what truly matters in the context of asymptotic analysis is that a particular parameter stays finite while another parameter assumes its asymptotic value.

Case	Description	Consequences
1	$b \to \infty$; $\sin\phi = 1$	$\upsilon = b \to \infty$
2	$b \to 0$; $\sin\phi = 1$	$\upsilon = b \to 0$
3	$\sin\phi \to 0$; $b = 1$	$\upsilon = \sin\phi \to 0$

Table 2: Limiting cases for 2D elements

The two main volume metrics for 2D elements are

$$\begin{aligned} \mu_{56,v} &= \frac{1}{2}\left(\upsilon + \frac{1}{\upsilon}\right) - 1, \\ \mu_{77,v} &= \frac{1}{2}\left(\upsilon^2 + \frac{1}{\upsilon^2}\right) - 1. \end{aligned}$$

The asymptotic limits of the volume metrics are given in Table 3.

Case	$\mu_{56,v}$	$\mu_{77,v}$
1	$\frac{\upsilon}{2}$	$\frac{\upsilon^2}{2}$
2	$\frac{1}{2\upsilon}$	$\frac{1}{2\upsilon^2}$
3	$\frac{1}{2\upsilon}$	$\frac{1}{2\upsilon^2}$

Table 3: Asymptotic Forms of the 2D Volume Metrics

Two of the main shape metrics are

$$\begin{aligned} \mu_{2,s} &= \frac{|A|^2}{2\,det(A)} - 1, \\ \mu_{50,s} &= \frac{|A^tA|^2}{2\,[det(A)]^2} - 1. \end{aligned}$$

Using the definitions above, the two shape metrics can be expressed in terms of the geometric parameters as

$$\begin{aligned} \mu_{2,s} &= \frac{1+b^2}{2\,b\,\sin\phi} - 1, \\ \mu_{50,s} &= \frac{1+2\,b^2\cos^2\phi + b^4}{2\,b^2\sin^2\phi} - 1. \end{aligned}$$

Table 4 shows the asymptotic limits of the two shape metrics for the three Cases.

Case	$\mu_{2,s}$	$\mu_{50,s}$
1	$\frac{\upsilon}{2}$	$\frac{\upsilon^2}{2}$
2	$\frac{1}{2\upsilon}$	$\frac{1}{2\upsilon^2}$
3	$\frac{1}{\upsilon}$	$\frac{2}{\upsilon^2}$

Table 4: Asymptotic Forms of the 2D Shape Metrics

Putting this all together, for $\mu_{2,s}$ and $\mu_{56,v}$ we have the results in Table 5. The two metrics cannot be asymptotically balanced with the same compound metric covering all three cases, but as a compromise, metric $\mu_{94,vs} = \mu_{2,s} + \lambda\,\mu_{56,v}$ is suggested, with $1 \le \lambda \le 2$. Note that this is a re-definition of the original metric 94. Also note that we don't form a convex combination of the metrics as in (1.1), as this is not required for any theoretical or practical purposes.

Case	$\mu_{2,s}$	$\mu_{56,v}$	Relation
1	$\frac{\upsilon}{2}$	$\frac{\upsilon}{2}$	$\mu_{56,v} = \mu_{2,s}$
2	$\frac{1}{2\upsilon}$	$\frac{1}{2\upsilon}$	$\mu_{56,v} = \mu_{2,s}$
3	$\frac{1}{\upsilon}$	$\frac{1}{2\upsilon}$	$\mu_{56,v} = \frac{\mu_{2,s}}{2}$

Table 5: Suggested Compound Metric for the Combination of $\mu_{2,s}$ and $\mu_{56,v}$ is $\mu_{94,vs} = \mu_{2,s} + \lambda\,\mu_{56,v}$, with $1 \le \lambda \le 2$.

For the combination of $\mu_{2,s}$ and $\mu_{77,v}$ we have the results in Table 6. Note that the shape metric must be squared. (From previous work $\mu_{2,s}^2 = \mu_{30,s}$.) Compound metrics that use a nonlinear combination will be denoted by an overline.

Figure 3 shows the optimal mesh produced by the compound metric $\mu_{2,s} + 1.5\,\mu_{56,v}$ based on the asymptotic analysis above. Note that the final λ value is

Case	$\mu_{2,s}$	$\mu_{77,v}$	Relation
1	$\frac{v}{2}$	$\frac{v^2}{2}$	$\mu_{77,v} = 2\,\mu_{2,s}^2$
2	$\frac{1}{2\,v}$	$\frac{1}{2\,v^2}$	$\mu_{77,v} = 2\,\mu_{2,s}^2$
3	$\frac{1}{v}$	$\frac{1}{2\,v^2}$	$\mu_{77,v} = \frac{1}{2}\mu_{2,s}^2$

Table 6: Suggested Compound Metric for the combination of $\mu_{2,s}$ and $\mu_{77,v}$ is $\overline{\mu_{80,vs}} = \mu_{2,s}^2 + \lambda\,\mu_{77,v}$, with $\frac{1}{2} \leq \lambda \leq 2$.

chosen as the average value of the admissible range from Table 5. Figure 4 shows the optimal mesh produced by the compound metric $\mu_{2,s}^2 + 1.25\mu_{77,v}$ based on Table 6. Both results have well-balanced shape and area.

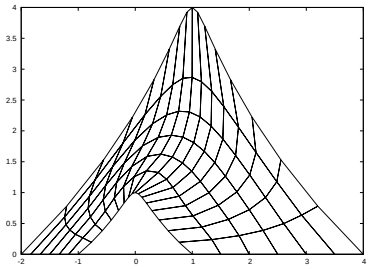

Figure 3: Optimal Mesh from $\mu_{2,s} + 1.5\,\mu_{56,v}$.

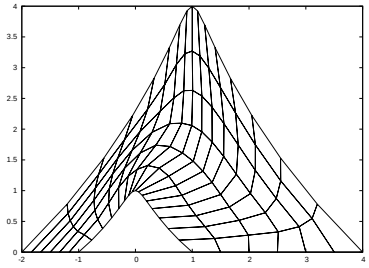

Figure 4: Optimal Mesh from $\mu_{2,s}^2 + 1.25\mu_{77,v}$.

For the combination $\mu_{50,s}$ and $\mu_{56,v}$ we have the results in Table 7. For the combination $\mu_{50,s}$ and $\mu_{77,v}$ we have the results in Table 8.

Figure 5 shows the optimal mesh produced by the compound metric $\mu_{50,s} + 2\,\mu_{56,v}^2$ based on Table 7, where λ is chosen as the minimum of the range. Figure 6 shows the optimal mesh produced by the compound metric $\mu_{50,s} + 4\,\mu_{77,v}^2$ based on Table 8, where λ is chosen as the maximum of the range. In both cases the optimized meshes have well-balanced shape and area.

From this analysis, it appears that $\mu_{56,v}$ is best combined with $\mu_{2,s}$ while $\mu_{77,v}$ is best combined with $\mu_{50,s}$, as the resulting compound metrics are linear combinations of shape and volume metrics. Since the analysis only provides an admissible range for λ, instead of an exact value, we recommend to use the average of the range to achieve balance between the different asymptotic limits. Similar asymptotic analysis can be performed for other combinations of shape and volume metrics.

Case	$\mu_{50,s}$	$\mu_{56,v}$	Relation
1	$\frac{v^2}{2}$	$\frac{v}{2}$	$\mu_{50,s} = 2\,\mu_{56,v}^2$
2	$\frac{1}{2\,v^2}$	$\frac{1}{2\,v}$	$\mu_{50,s} = 2\,\mu_{56,v}^2$
3	$\frac{2}{v^2}$	$\frac{1}{2\,v}$	$\mu_{50,s} = 8\,\mu_{56,v}^2$

Table 7: Suggested Compound Metric for the combination of $\mu_{50,s}$ and $\mu_{56,v}$ is $\overline{\mu_{53,sv}} = \mu_{50,s} + \lambda\,\mu_{56,v}^2$, with $2 \leq \lambda \leq 8$.

Case	$\mu_{50,s}$	$\mu_{77,v}$	Relation
1	$\frac{v^2}{2}$	$\frac{v^2}{2}$	$\mu_{50,s} = \mu_{77,v}$
2	$\frac{1}{2\,v^2}$	$\frac{1}{2\,v^2}$	$\mu_{50,s} = \mu_{77,v}$
3	$\frac{2}{v^2}$	$\frac{1}{2\,v^2}$	$\mu_{50,s} = 4\,\mu_{77,v}$

Table 8: Suggested Compound Metric for the Combination of $\mu_{50,s}$ and $\mu_{77,v}$ is $\mu_{90,sv} = \mu_{50,s} + \lambda\,\mu_{77,v}$, with $1 \leq \lambda \leq 4$.

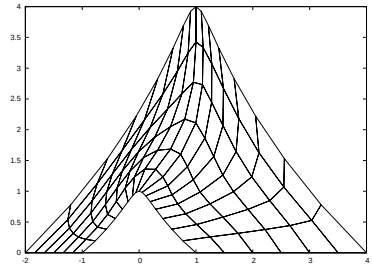

Figure 5: Optimal Meshes from $\mu_{50,s} + 2\,\mu_{56,v}^2$.

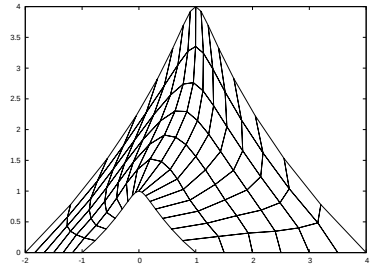

Figure 6: Optimal Meshes from $\mu_{50,s} + 4\,\mu_{77,v}^2$.

2.1 Incorporating the Target Matrix The analysis above assumed that the target matrix was $W = I$.

We consider next the more appropriate target

$$W = \sqrt{\bar{v}}\, I,$$

where $\bar{v}$ is the user-specified target local volume. This target is commonly used when we want ideal shape, but local volume is a constant based on the area of the domain and the number of elements. The constant $\bar{v}$ is that averaged local area over the domain. For this target we have $T = A\, W^{-1}$, giving

$$T = \frac{1}{\sqrt{\bar{v}}} \begin{pmatrix} 1 & b\cos\phi \\ 0 & b\sin\phi \end{pmatrix},$$

so that $\tau = \frac{v}{\bar{v}}$ and $|\ T\ |^2 = \frac{1+b^2}{\bar{v}}$. For the metrics $\mu_{2,s}(T)$ and $\mu_{56,v}(T)$ we have

$$\begin{aligned} \mu_{2,s}(T) &= \frac{1+b^2}{2\,v} - 1, \\ \mu_{56,v}(T) &= \frac{1}{2}\left(\frac{v}{\bar{v}} + \frac{\bar{v}}{v}\right) - 1. \end{aligned}$$

Importantly, $\mu_{2,s}$, being a shape metric, is invariant to $\bar{v}$ while the volume metric is not invariant. Table 9 shows the limiting behavior of $\mu_{2,s}(T)$ and $\mu_{56,v}(T)$. The asymptotic balance between the two metrics varies over the three cases, but the basic compound metric is $\mu_{2,s} + \lambda\,\mu_{56,v}$. If $\bar{v} > 1$, then $\frac{1}{\bar{v}} \le \lambda \le \bar{v}$. In that case, a good compromise value of λ is perhaps $\lambda = 1$. On the other hand, if $\bar{v} < 1$, we have $\bar{v} \le \lambda \le \frac{2}{\bar{v}}$. Thus, $\lambda = 1$ is again a good compromise over the three cases.

Case	$\mu_{2,s}$	$\mu_{56,v}$	Relation
1	$\frac{v}{2}$	$\frac{v}{2\,\bar{v}}$	$\mu_{2,s} = \bar{v}\,\mu_{56,v}$
2	$\frac{1}{2\,v}$	$\frac{\bar{v}}{2\,v}$	$\mu_{2,s} = \frac{\mu_{56,v}}{\bar{v}}$
3	$\frac{1}{v}$	$\frac{\bar{v}}{2\,v}$	$\mu_{2,s} = \frac{2\,\mu_{56,v}}{\bar{v}}$

Table 9: Suggested Compound Metric for the Combination of $\mu_{2,s}$ and $\mu_{56,v}$ with Target $W = \sqrt{\bar{v}}\, I$ is $\mu_{2,s} + \lambda\,\mu_{56,v}$ with $\min\left(\frac{1}{v}, \bar{v}\right) \le \lambda \le \max\left(\frac{2}{\bar{v}}, \bar{v}\right)$.

A similar analysis holds for the other combinations of shape and volume metrics. It thus seems that including $\bar{v}$ in the compound metric is not really necessary to achieve a compromise asymptotic balance.

3 Compound Metrics for 3D Elements

In 3D the Jacobian matrix depends on three lengths (ℓ_1, ℓ_2, ℓ_3) and three angles (ϕ, ψ, χ). Again we assume $W = I$, i.e, $T = A$ and $\tau = v$, to simplify the presentation of the main idea. We can write $A = R\,U$, where R controls the orientation, but since VS metrics are invariant to orientation we can set $R = I$ and therefore $A = U$, with

$$U = \begin{pmatrix} \ell_1 & \ell_2\cos\phi & \ell_3\cos\psi \\ 0 & \ell_2\sin\phi & \ell_3\sin\psi\cos\chi \\ 0 & 0 & \ell_3\sin\psi\sin\chi \end{pmatrix},$$

where $0 < \phi, \psi, \chi < \pi$. The determinant gives

$$v = \zeta\,\sin\phi\sin\psi\sin\chi,$$

with $\zeta = \ell_1\,\ell_2\,\ell_3$. With no loss of generality, we set $\ell_1 = 1$. Also let $\ell_2 = a$ and $\ell_3 = b$ for simplicity. This gives A in terms of five parameters a, b, ϕ, ψ, χ

$$A = \begin{pmatrix} 1 & a\cos\phi & b\cos\psi \\ 0 & a\sin\phi & b\sin\psi\cos\chi \\ 0 & 0 & b\sin\psi\sin\chi \end{pmatrix},$$

with

$$det(A) = v = a\,b\,\sin\phi\sin\psi\sin\chi.$$

The Euclidean norm (squared) of A is thus

$$|\ A\ |^2 = 1 + a^2 + b^2.$$

In addition, with $\mathcal{CS} := \cos\phi\sin\psi$, the adjugate of A is

$$adj\ A = \begin{pmatrix} v & -a\,b\,\mathcal{CS}\sin\chi & a\,b\,(\mathcal{CS}\cos\chi - \sin\phi\cos\psi) \\ 0 & b\sin\psi\sin\chi & -b\,\sin\psi\cos\chi \\ 0 & 0 & a\,\sin\phi \end{pmatrix}.$$

Thus

$$\begin{aligned} |\ adj\ A\ |^2 &= a^2\sin^2\phi + b^2\sin^2\psi \\ &+ a^2b^2(\cos\phi\sin\psi\cos\chi - \sin\phi\cos\psi)^2 \\ &+ a^2b^2\sin^2\psi\sin^2\chi. \end{aligned}$$

Table 10 describes various 3D limiting cases. Given these seven limiting cases, we calculate in Table 11 the limiting values of $|\ A\ |^2$, $|\ adj\ A\ |^2$, and v.

Case	a	b	$\sin\phi$	$\sin\psi$	$\sin\chi$
1	1	1	1	1	$\to 0$
2	1	1	1	$\to 0$	1
3	1	1	$\to 0$	1	1
4	$\to \infty$	1	1	1	1
5	$\to 0$	1	1	1	1
6	1	$\to \infty$	1	1	1
7	1	$\to 0$	1	1	1

Table 10: Limiting Cases for 3D Jacobian

Case	$\mid A \mid^2$	$\mid adj\ A \mid^2$	υ
1	3	2	$\to 0$
2	3	2	$\to 0$
3	3	2	$\to 0$
4	$\to a^2$	$2\,a^2$	$\to a$
5	2	1	$\to 0$
6	$\to b^2$	$2\,b^2$	$\to b$
7	2	1	$\to 0$

Table 11: Limiting behavior of $\mid A \mid^2$, $\mid adj\ A \mid^2$, and υ

Case	υ	$\mu_{316,\upsilon}$	$\mu_{318,\upsilon}$
1	$\to 0$	$\frac{1}{2\,\upsilon}$	$\frac{1}{2\,\upsilon^2}$
2	$\to 0$	$\frac{1}{2\,\upsilon}$	$\frac{1}{2\,\upsilon^2}$
3	$\to 0$	$\frac{1}{2\,\upsilon}$	$\frac{1}{2\,\upsilon^2}$
4	$\to a$	$\frac{\upsilon}{2}$	$\frac{\upsilon^2}{2}$
5	$\to 0$	$\frac{1}{2\,\upsilon}$	$\frac{1}{2\,\upsilon^2}$
6	$\to b$	$\frac{\upsilon}{2}$	$\frac{\upsilon^2}{2}$
7	$\to 0$	$\frac{1}{2\,\upsilon}$	$\frac{1}{2\,\upsilon^2}$

Table 12: Limiting Cases for $\mu_{316,\upsilon}$ and $\mu_{318,\upsilon}$

The two main volume metrics in 3D are

$$\begin{aligned}\mu_{316,\upsilon} &= \frac{1}{2}\left(\sqrt{\upsilon} - \frac{1}{\sqrt{\upsilon}}\right)^2 = \frac{1}{2}\left(\upsilon + \frac{1}{\upsilon}\right) - 1,\\ \mu_{318,\upsilon} &= \frac{1}{2}\left(\upsilon - \frac{1}{\upsilon}\right)^2 = \frac{1}{2}\left(\upsilon^2 + \frac{1}{\upsilon^2}\right) - 1.\end{aligned}$$

We calculate their asymptotic behavior in Table 12. The major shape metrics in 3D are

$$\begin{aligned}\mu_{301,s} &= \frac{1}{3} \mid A \mid \mid adj\ A \mid -1,\\ \mu_{302,s} &= \frac{1}{9} \mid A \mid^2 \mid adj\ A \mid^2 -1,\\ \mu_{303,s} &= \frac{\mid A \mid^2}{3\upsilon^{2/3}} - 1,\\ \mu_{304,s} &= \frac{\mid A \mid^3}{3\sqrt{3}\,\upsilon} - 1.\end{aligned}$$

Next, we try to match the growth rates of the shape metrics with the two volume metrics. Table 14 gives the results for $\mu_{304,s}$ when combined with either $\mu_{316,\upsilon}$ or $\mu_{318,\upsilon}$. It is not possible to match the shape and volume metrics in the asymptotic limit over the seven cases. As a compromise we give two compound metrics in the *All* row, both with $1 \le p \le 2$ and $0.77 \le \lambda \le 2$. It is also not possible to nicely match the asymptotic volume metrics with $\mu_{303,s}$ (see Table 15).

It is possible, however, to obtain reasonable matches

Case	$\mu_{301,s}$	$\mu_{302,s}$	$\mu_{303,s}$	$\mu_{304,s}$
1	$\frac{\sqrt{6}}{3\,\upsilon}$	$\frac{2}{3\,\upsilon^2}$	$\frac{1}{\upsilon^{2/3}}$	$\frac{1}{\upsilon}$
2	$\frac{\sqrt{6}}{3\,\upsilon}$	$\frac{2}{3\,\upsilon^2}$	$\frac{1}{\upsilon^{2/3}}$	$\frac{1}{\upsilon}$
3	$\frac{\sqrt{6}}{3\,\upsilon}$	$\frac{2}{3\,\upsilon^2}$	$\frac{1}{\upsilon^{2/3}}$	$\frac{1}{\upsilon}$
4	$\frac{\sqrt{2}\,\upsilon}{3}$	$\frac{2\,\upsilon^2}{9}$	$\frac{\upsilon^{4/3}}{3}$	$\frac{\upsilon^2}{3\sqrt{3}}$
5	$\frac{\sqrt{2}}{3\,\upsilon}$	$\frac{2}{9\,\upsilon^2}$	$\frac{2}{3\,\upsilon^{2/3}}$	$\left(\frac{2}{3}\right)^{\frac{3}{2}} \cdot \frac{1}{\upsilon}$
6	$\frac{\sqrt{2}\,\upsilon}{3}$	$\frac{2\,\upsilon^2}{9}$	$\frac{\upsilon^{4/3}}{3}$	$\frac{\upsilon^2}{3\sqrt{3}}$
7	$\frac{\sqrt{2}}{3\,\upsilon}$	$\frac{2}{9\,\upsilon^2}$	$\frac{2}{3\,\upsilon^{2/3}}$	$\left(\frac{2}{3}\right)^{\frac{3}{2}} \cdot \frac{1}{\upsilon}$

Table 13: Limiting Cases for the 3D Shape Metrics

for the volume metrics with the asymptotic forms of $\mu_{302,s}$ (Table 16) and $\mu_{301,s}$ (Table 17).

4 Theory of Compound Metrics

Having analyzed the asymptotic situation for various specific compound metrics in both 2D and 3D, we take a slightly more general view in this section in which we consider compound metrics that are general functions of pairs of subordinate metrics. Let μ_x and μ_y be any two distinct subordinate metrics. Then we shall study compound metrics of the form $F = F(x, y)$ with $x = \mu_x$ and $y = \mu_y$. Some examples of such functions are

$$F_1(x, y) = (1 - \gamma)\, x + \gamma\, y,$$

with $\gamma \in (0, 1)$, and the functions from sections 1 and 2:

$$\begin{aligned}F_2(x, y) &= x + \lambda\, y,\\ F_3(x, y) &= x^2 + \lambda\, y,\\ F_4(x, y) &= x + \lambda\, y^2,\end{aligned}$$

with λ a constant. There are, of course, many additional functions that can be considered, some considerably more exotic than these. The first goal then is to identify the properties F needs to have in order that an optimal mesh can be found by minimizing $F(x, y)$. Recall that the subordinate metrics are assumed to be non-negative. Let $F : \mathcal{D}^2 \to \mathcal{D}$ with

$$\begin{aligned}\mathcal{D} &\equiv \{x \in \Re \mid x \ge 0\},\\ \mathcal{D}^2 &\equiv \mathcal{D} \times \mathcal{D},\\ \hat{\mathcal{D}}^2 &\equiv \mathcal{D}^2 \setminus \{(0, 0)\}.\end{aligned}$$

We want to minimize $\hat{\mu} = F(\mu_x, \mu_y)$ as a function of T and ultimately, as a function of the mesh nodal coordinates. We have $\hat{\mu}(T) = F(\mu_x(T), \mu_y(T))$. We require F to satisfy a number of properties so that this minimization problem can produce decent optimal

Cases	$\mu_{304,s}$	$\mu_{316,v}$	Compound	$\mu_{318,v}$	Compound
1, 2, 3	$\frac{1}{v}$	$\frac{1}{2\,v}$	$\mu_{304,s} + 2\,\mu_{316,v}$	$\frac{1}{2\,v^2}$	$\mu_{304,s}^2 + 2\,\mu_{318,v}$
4, 6	$\frac{v^2}{3\sqrt{3}}$	$\frac{v}{2}$	$\mu_{304,s} + \left(\frac{4}{3\sqrt{3}}\right)\,\mu_{316,v}^2$	$\frac{v^2}{2}$	$\mu_{304,s} + \left(\frac{2}{3\sqrt{3}}\right)\,\mu_{318,v}$
5, 7	$\left(\frac{2}{3}\right)^{\frac{3}{2}} \cdot \frac{1}{v}$	$\frac{1}{2\,v}$	$\mu_{304,s} + 2\,\left(\frac{2}{3}\right)^{\frac{3}{2}}\,\mu_{316,v}$	$\frac{1}{2\,v^2}$	$\mu_{304,s}^2 + 2\,\left(\frac{2}{3}\right)^3\,\mu_{318,v}$
All			$\mu_{304,s} + \lambda\,\mu_{316,v}^p$		$\mu_{304,s}^p + \lambda\,\mu_{318,v}$

Table 14: Compound Metrics for $\mu_{304,s}$. It is not possible to match the shape and volume asymptotic limits over all cases.

Cases	$\mu_{303,s}$	$\mu_{316,v}$	Compound	$\mu_{318,v}$	Compound
1, 2, 3	$\frac{1}{v^{2/3}}$	$\frac{1}{2\,v}$	$\mu_{303,s} + \left(2\,\mu_{316,v}\right)^{2/3}$	$\frac{1}{2\,v^2}$	$\mu_{303,s}^3 + 2\,\mu_{318,v}$
4, 6	$\frac{v^{4/3}}{3}$	$\frac{v}{2}$	$3\,\mu_{303,s} + \left(2\,\mu_{316,v}\right)^{4/3}$	$\frac{v^2}{2}$	$\left(3\,\mu_{303,s}\right)^{3/2} + 2\,\mu_{318,v}$
5, 7	$\frac{2}{3\,v^{2/3}}$	$\frac{1}{2\,v}$	$\frac{3}{2}\,\mu_{303,s} + \left(2\,\mu_{316,v}\right)^{2/3}$	$\frac{1}{2\,v^2}$	$\left(\frac{3}{2}\,\mu_{303,s}\right)^3 + 2\,\mu_{318,v}$
All			$\lambda\,\mu_{303,s} + \left(2\,\mu_{316,v}\right)^p$		$\left(\lambda\,\mu_{303,s}\right)^p + 2\,\mu_{318,v}$

Table 15: Compound Metrics for $\mu_{303,s}$. It is not possible to match the shape and volume asymptotic limits over all cases.

meshes when μ_x and μ_y do. Assuming that μ_x and μ_y are good optimization metrics, the minimal properties that we believe F needs are

1. $F(x, y)$ is continuous on $\mathcal{D}^2$,
2. $F(x, y) = 0$ if and only if $(x, y) = (0, 0)$,
3. F has no stationary points on $\mathcal{D}^2$ except possibly at $(0, 0)$.

Preferably, F will not only be continuous, but twice differentiable so that gradient and Hessian-based numerical optimization methods can be used. Because the range of F is $\mathcal{D}$, criterion 2 means that the set of global minimizers $\mathcal{G}_{\hat{\mu}}$ of $\hat{\mu}(T)$ consists of those points in $\mathcal{G}_{\mu_x} \cap \mathcal{G}_{\mu_y}$.
Criterion 3 can be replaced by the condition that

$$x\,\frac{\partial F}{\partial x} + y\,\frac{\partial F}{\partial y} > 0$$

on $\hat{\mathcal{D}}^2$. This condition says that the function value must decrease as one moves directly toward $(0, 0)$. Notice that if this condition holds, the two partial derivatives at any given point cannot both be negative (or non-positive). The derivative of $\hat{\mu}$ with respect to the matrix T is

$$\frac{\partial \hat{\mu}}{\partial T} = \frac{\partial F}{\partial \mu_x}\frac{\partial \mu_x}{\partial T} + \frac{\partial F}{\partial \mu_y}\frac{\partial \mu_y}{\partial T},$$

with μ_x and μ_y specific subordinate metrics. Let $\mathcal{S}_{\hat{\mu}}$ denote the set of stationary points of $\hat{\mu}$. The stationary point equation of $\hat{\mu}$ is thus

$$\frac{\partial F}{\partial \mu_x}\frac{\partial \mu_x}{\partial T} + \frac{\partial F}{\partial \mu_y}\frac{\partial \mu_y}{\partial T} = 0.$$

From this, it is clear that if $T \in \mathcal{S}_{\mu_x} \cap \mathcal{S}_{\mu_y}$, then T is a stationary point of $\hat{\mu}$.
Proposition. If $\frac{\partial \mu_x}{\partial T}$ and $\frac{\partial \mu_y}{\partial T}$ are linearly independent, then $\mathcal{S}_{\hat{\mu}} = \mathcal{S}_{\hat{\mu}_x} \cap \mathcal{S}_{\mu_y}$.
Proof. The set of 2×2 (or 3×3) matrices forms a vector space. Thus any linear combination of linearly independent matrices is zero only if the two matrices are both zero or if the coefficients in the linear combination are all zero. But criterion 3 above precludes the latter possibility, so the two matrices must be zero. That means any stationary point of $\hat{\mu}$ must belong to the intersection of the set of stationary points of the two subordinate metrics. §

4.1 The Path of Iteration Motivated by the above discussion, in this subsection we propose a new approach for minimizing compound metrics, based on the sign of their derivatives.

The mesh optimization procedure used to create the optimal mesh is generally iterative. Let the iteration counter be n, with $0 \le n \le N$. Correspondingly, there is a sequence of meshes that converge towards the optimal mesh. The metrics $x = \mu_x$ and $y = \mu_y$ vary with n and with the sample point. Define $(\bar{x}_n, \bar{y_n}) \in \mathcal{D}^2$ to be a sequence of points given by the average of each metric over the sample points at each iteration. We call this sequence of points the *path of iteration*. The path starts at the point $(\bar{x}_o, \bar{y}_o)$ and ends at the point $(\bar{x}_N, \bar{y}_N)$. In general, the final point $(\bar{x}_N, \bar{y}_N) \neq (0, 0)$ due to the constraints imposed by the fixed mesh connectivity and fixed boundary nodes.

Cases	$\mu_{302,s}$	$\mu_{316,v}$	Compound	$\mu_{318,v}$	Compound
1, 2, 3	$\frac{2}{3\,v^2}$	$\frac{1}{2\,v}$	$\frac{3}{8}\,\mu_{302,s} + \mu_{316,v}^2$	$\frac{1}{2\,v^2}$	$\mu_{302,s} + 3\,\mu_{318,v}$
4, 6	$\frac{2\,v^2}{9}$	$\frac{v}{2}$	$\frac{9}{8}\,\mu_{302,s} + \mu_{316,v}^2$	$\frac{v^2}{2}$	$\mu_{302,s} + \frac{4}{9}\,\mu_{318,v}$
5, 7	$\frac{2}{9\,v^2}$	$\frac{1}{2\,v}$	$\frac{9}{8}\,\mu_{302,s} + \mu_{316,v}^2$	$\frac{1}{2\,v^2}$	$\mu_{302,s} + \frac{4}{9}\,\mu_{318,v}$
All			$\lambda\,\mu_{302,s} + \mu_{316,v}^2$		$\mu_{302,s} + \lambda\,\mu_{318,v}$

Table 16: Compound Metrics for $\mu_{302,s}$. Suggested Compound Metric is $\mu_{338,vs} = \mu_{302,s} + \lambda\,\mu_{318,v}$, with $\frac{4}{9} \le \lambda \le 3$.

Cases	$\mu_{301,s}$	$\mu_{316,v}$	Compound	$\mu_{318,v}$	Compound
1, 2, 3	$\frac{\sqrt{6}}{3\,v}$	$\frac{1}{2\,v}$	$\frac{3}{8}\,\mu_{301,s} + \mu_{316,v}$	$\frac{1}{2\,v^2}$	$\mu_{301,s}^2 + \frac{4}{3}\,\mu_{318,v}$
4, 6	$\frac{\sqrt{2}\,v}{3}$	$\frac{v}{2}$	$\frac{9}{8}\,\mu_{301,s} + \mu_{316,v}$	$\frac{v^2}{2}$	$\mu_{301,s}^2 + \frac{4}{9}\,\mu_{318,v}$
5, 7	$\frac{\sqrt{2}}{3\,v}$	$\frac{1}{2\,v}$	$\frac{9}{8}\,\mu_{301,s} + \mu_{316,v}$	$\frac{1}{2\,v^2}$	$\mu_{301,s}^2 + \frac{4}{9}\,\mu_{318,v}$
All			$\lambda\,\mu_{301,s} + \mu_{316,v}$		$\mu_{301,s}^2 + \lambda\,\mu_{318,v}$

Table 17: Compound Metrics for $\mu_{301,s}$. Suggested Compound Metric is $\mu_{370,vs} = \mu_{301,s} + \lambda\,\mu_{316,v}$, with $\frac{3}{8} \le \lambda \le \frac{9}{8}$.

In Figure 7 we show what the path of iteration looks like for the metric $\mu_{2,s} + 2\,\mu_{56,v}$ with $\bar{x} = \mu_{2,s}$ on the x-axis. The path starts at the upper right and proceeds to the lower left, ending in a fish-hook. This is a typical curve for the compound metrics: at first both the shape and volume metrics decrease in a linear fashion because the initial mesh was optimized for neither. At some point in the iteration, however, it becomes more difficult to make progress on both metrics simultaneously due to the constraint of mesh connectivity. In this particular example, the fishhook bends to the left as one moves along the path, indicating that no more progress can be made in shape improvement, while volume improvement can continue. On the fishhook portion of the curve then, volume is being improved while shape is getting worse. The resultant optimal mesh is shown in the bottom left of Figure 7. It took 80 iterations to reach convergence. Next, we implemented a scheme in our optimization code in which iterations are terminated, not only if the maximum distance-moved is less than some tolerance, but also if either $\bar{x}_n$ or $\bar{y}_n$ starts to increase. With that new termination criterion enabled, the optimization was repeated. Termination was reached after only 15 iterations and the optimal mesh is shown on bottom right part of the figure. In principle, with this early termination procedure, the path no longer has the fishhook and both shape and volume are continually decreased. The difference in the two optimal meshes is almost indiscernible.

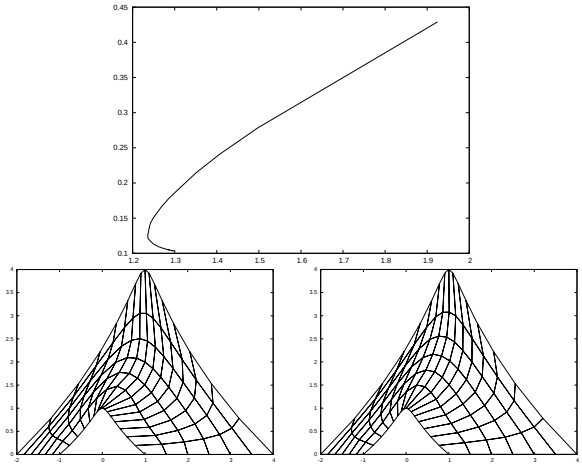

Figure 7: Top: iterative path of $F(x, y) = x + 2y$ for $x = \mu_{2,s}$ and $y = \mu_{56,v}$. Bottom: final optimized mesh after the full 80 iterations (left) and final optimized mesh after early termination with 15 iterations (right).

5 Application Examples

This section presents several user examples that utilize asymptotically balanced metrics. The mesh optimization computations are performed as part of multi-material Arbitrary Lagrangian-Eulerian (ALE) simulations [2, 1], where the mesh moves with the material velocity, but is being optimized periodically to improve its shape and adapt its local size [7]. Since both the shape quality and size adaptivity are important for the users, achieving appropriate balance is required for these simulations.

Before the introduction of the asymptotically balanced metrics, users had to adjust the parameter γ in (1.1) by trial and error. For different simulations, the optimal values of γ were often different by orders of

magnitude. Furthermore, it was difficult to say that an optimal value of γ existed even for a single ALE simulation, as the mesh optimization procedure is applied on different meshes with different levels of deformation. These challenges have been resolved by using asymptotically balanced metrics.

2D Shaped Charge The first example is a 2D shaped charge simulation. The goal of each mesh optimization stage is to obtain ideal shape (the shape target is the unit square), while adapting the mesh size to obtain better resolution at all material interfaces with ratio 3:1 (big size vs small size). The mesh positions stay fixed in those parts of the domain that have not experienced any material motion. Figure 8 presents results that use $\mu_{94,vs}$ with $\lambda = 1.5$ (see Table 5) for all mesh optimizations throughout the whole ALE simulation. The obtained meshes appear to be well balanced, with good shape quality and accurate size adaptation.

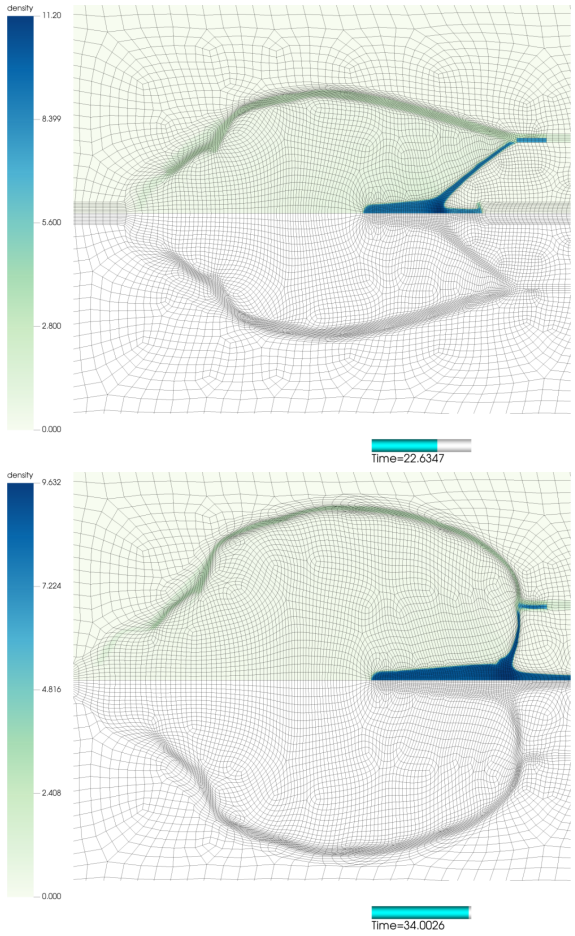

Figure 8: 2D shaped charge simulation: density and mesh positions at $t = 22.6$ and $t = 34$.

2D and 3D Ball Impact The second example is a 2D/3D high-velocity ball impact simulation. The goal of each mesh optimization stage is to obtain ideal shape (the shape target is the unit square), while adapting the mesh size to obtain better resolution in the regions occupied by the ball and the wall, with ratio 2:1 (big size vs small size). Figures 9 and 10 present 2D and 3D results, respectively, that use $\mu_{94,vs}$ (2D) and $\mu_{338,vs}$ (3D) for all mesh optimizations throughout the whole ALE simulation. Since the shape quality is critical to the robustness and time step size of the 3D simulation, more weight is put on the shape part of the VS metrics. This is achieved by scaling the default λ value by 0.1. While this scaling pushes the λ value beyond the admissible range (see Table 16), it serves as an illustration of customizing the default value to highlight the desired shape quality in an application-specific context. This results in $\lambda = 1.5$ for $\mu_{94,vs}$ (see Table 5), and $\lambda = 0.1 * \frac{1}{2}(\frac{4}{9} + 3)$ for $\mu_{338,vs}$ (see Table 16). The obtained meshes appear to be well balanced, with good shape quality and accurate size adaptation.

6 Conclusion

Asymptotic analysis of pairs of shape and volume metrics proves useful in determining the best form of the combined metrics. For the 2D elements, the two volume metrics are essentially based on τ ($\mu_{56,v}$) and τ^2 ($\mu_{77,v}$). One can obtain a linear compound metric of the form $F(x, y) = x + \lambda y$ by combining the former with shape metric $\mu_{2,s}$ and the latter with shape metric $\mu_{50,s}$. These give the compound metrics $\mu_{94,vs} = \mu_{2,s} + \lambda \mu_{56,v}$ and $\mu_{80,vs} = \mu_{50,s} + \lambda \mu_{77,v}$. In 3D, there are also pairings of shape and volume metrics which give a linear combination of metrics. From the present analysis, these would be $\mu_{370,vs} = \mu_{301,s} + \lambda \mu_{316,v}$ and $\mu_{338,vs} = \mu_{302,s} + \lambda \mu_{318,v}$. The values of λ in these compound metrics serve to compromise between the limiting asymptotic cases.

Of course, there is nothing wrong with using the non-linear compound metrics like $x^2 + \lambda y$ or $x + \lambda y^2$ either, particularly since these functions satisfy the criterion mentioned in Section 4. Those conditions guarantee, among other things, that if μ_s is a shape metric and μ_v is a volume metric, then $F(x, y)$ is a volume+shape (VS) metric. In addition, these new compound metrics are grade A metrics, based on the classification defined in [18], i.e., they can be shown to meet the seventeen criteria for a robust mesh optimization metric, see [18].

An asymptotic analysis which explicitly included the target-matrix revealed that doing so only serves to broaden the interval in which λ belongs. A compromise value, such as $\lambda = 1$, shows that we do not even need to take the target into account, at least not for constant

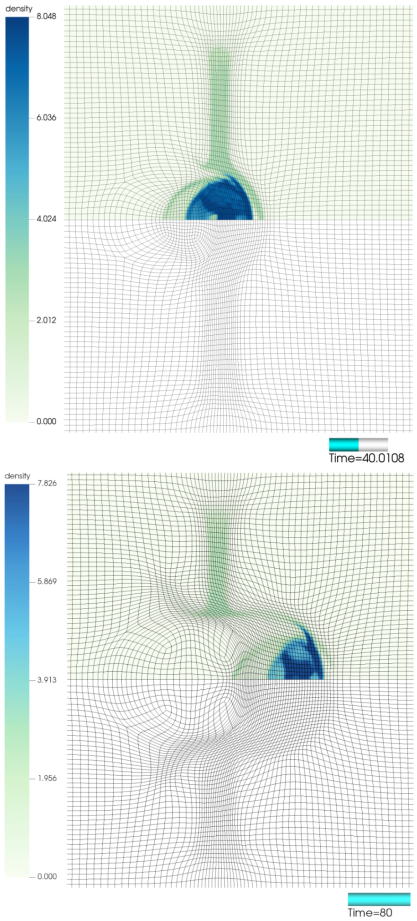

Figure 9: 2D ball impact simulation: density and mesh positions at $t = 40$ and $t = 80$.

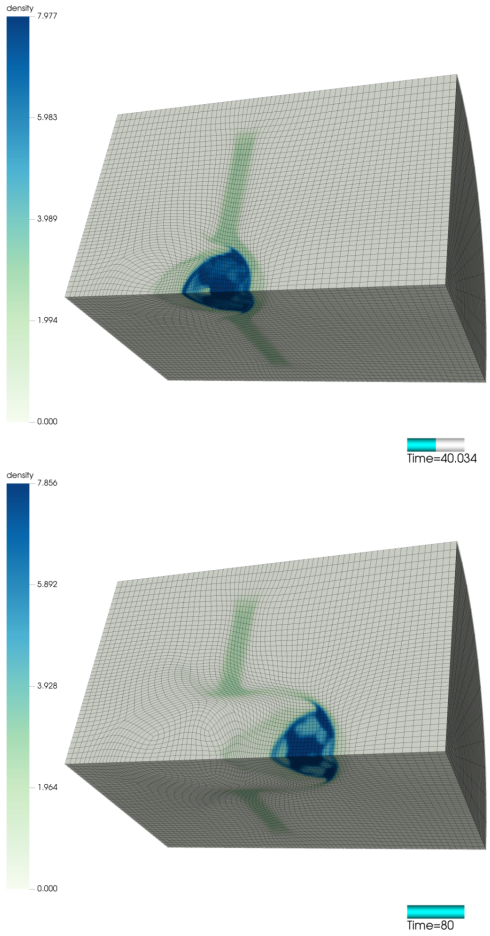

Figure 10: 3D ball impact simulation: density and mesh positions at $t = 40$ and $t = 80$.

targets. There could be an issue for spatially varying targets, but this is not investigated here.

Finally, Section 4.1 showed that it might be worthwhile to implement an early termination criterion for compound metrics based on whether μ_x or mu_y starts to increase during the iteration procedure. At worse, this could save a lot of unnecessary iterations and, at best, it might also give somewhat better looking optimal meshes than if the iterations are not terminated early.

References

[1] R. Anderson, A. Black, L. Busby, R. B. B. Blakeley, J.-S. Camier, J. Ciurej, V. D. A. Cook, N. Elliott, J. Grondalski, R. H. C. Harrison, T. Kolev, M. Legendre, W. N. W. Liu, B. Olson, M. Osawe, O. P. G. Papadimitrou, R. Pember, A. Skinner, T. S. D. Stevens, L. Taylor, V. Tomov, A. V. R. Rieben, K. Weiss, and D. White., *The multiphysics on advanced platforms project*, Tech. Rep. LLNL-TR-815869, Lawrence Livermore National Lab.(LLNL), Livermore, CA, 2020.

[2] R. W. Anderson, V. A. Dobrev, T. V. Kolev, R. N. Rieben, and V. Z. Tomov, *High-order multi-material ALE hydrodynamics*, SIAM J. Sci. Comp., 40 (2018), pp. B32–B58.

[3] G. Aparicio-Estrems, A. Gargallo-Peiró, and X. Roca, *Defining a stretching and alignment aware quality measure for linear and curved 2D meshes*, 27th International Meshing Roundtable, Springer International Publishing, 2019, pp. 37–55.

[4] ———, *Combining high-order metric interpolation and geometry implicitization for curved r-adaption*, Comput.-Aided Des., 157 (2023), p. 103478.

[5] ———, *Defining metric-aware size-shape measures to validate and optimize curved high-order meshes*, Comput.-Aided Des., 168 (2024), p. 103667.

[6] J. Castillo, S. Steinberg, and P. J. Roache, *Parameter estimation in variational grid generation*,

Applied Mathematics and Computation, 28 (1988), pp. 155–177.
[7] V. A. Dobrev, P. Knupp, T. V. Kolev, K. Mittal, R. N. Rieben, and V. Z. Tomov, *Simulation-driven optimization of high-order meshes in ALE hydrodynamics*, Comput. Fluids, 208 (2020), p. 104602.
[8] V. A. Dobrev, P. Knupp, T. V. Kolev, K. Mittal, and V. Z. Tomov, *The Target-Matrix Optimization Paradigm for high-order meshes*, SIAM J. Sci. Comp., 41 (2019), pp. B50–B68.
[9] P. Frey and F. Alauzet, *Anisotropic mesh adaptation for CFD computations*, Comput. Methods Appl. Mech. Eng., 194 (2005), pp. 5068–5082.
[10] A. Gargallo-Peiró, X. Roca, J. Peraire, and J. Sarrate, *Distortion and quality measures for validating and generating high-order tetrahedral meshes*, Eng. Comput., 31 (2015), pp. 423–437.
[11] P. T. Greene, S. P. Schofield, and R. Nourgaliev, *Dynamic mesh adaptation for front evolution using discontinuous Galerkin based weighted condition number relaxation*, J. Comput. Phys., 335 (2017), pp. 664–687.
[12] A. Johnen, C. Geuzaine, T. Toulorge, and J.-F. Remacle, *Efficient computation of the minimum of shape quality measures on curvilinear finite elements*, Comput.-Aided Des., 103 (2018), pp. 24–33.
[13] P. Knupp, *Algebraic mesh quality metrics*, SIAM J. Sci. Comp., 23 (2001), pp. 193–218.
[14] ———, *Introducing the target-matrix paradigm for mesh optimization by node movement*, Engineering with Computers, 28 (2012), pp. 419–429.
[15] P. Knupp, *Metric type in the target-matrix mesh optimization paradigm*, Tech. Rep. LLNL-TR-817490, Lawrence Livermore National Lab.(LLNL), Livermore, CA, 2020.
[16] ———, *Geometric parameters in the target matrix mesh optimization paradigm*, Partial Differ. Equations Appl. Math., 5 (2022), p. 100390.
[17] ———, *A target construction methodology for mesh quality improvement*, Eng. Comput., 38 (2022), pp. 4451–4474.
[18] ———, *Seventeen criteria for evaluating Jacobian-based optimization metrics*, Eng. Comput., 38 (2023).
[19] J. Marcon, , M. Turner, D. Moxey, S. Sherwin, and J. Peiro, *A variational approach to high-order r-adaptation*, 26th International Meshing Roundtable, Springer International Publishing, 2017.
[20] E. Ruiz-Gironés, X. Roca, and J. Sarrate, *Combining Size-Preserving and Smoothing Procedures for Adaptive Quadrilateral Mesh Generation*, Proceedings of the 22nd International Meshing Roundtable, Springer International Publishing, 2014, pp. 19–37.
[21] E. Ruiz-Gironés, X. Roca, and J. Sarrate, *High-order mesh curving by distortion minimization with boundary nodes free to slide on a 3D CAD representation*, Computer-Aided Design, 72 (2016), pp. 52–64.
[22] T. Toulorge, J. Lambrechts, and J.-F. Remacle, *Optimizing the geometrical accuracy of curvilinear meshes*, J. Comput. Phys., 310 (2016), pp. 361–380.
[23] M. Turner, J. Peiró, and D. Moxey, *Curvilinear mesh generation using a variational framework*, Computer-Aided Design, 103 (2018), pp. 73–91.